

---

# Model Hierarchy Based Optimal Control of Radiative Heat Transfer

---

Debora Clever<sup>1,2</sup>, Jens Lang<sup>1,2,3</sup> and Dirk Schröder<sup>2</sup>

<sup>1</sup>Graduate School CE, Technische Universität Darmstadt, Dolivostr. 15, D-64293 Darmstadt, Germany,

<sup>2</sup>Department of Mathematics, Technische Universität Darmstadt, Dolivostr. 15, D-64293 Darmstadt, Germany

<sup>3</sup>Center of Smart Interfaces, Technische Universität Darmstadt, Petersenstr. 30, D-64287 Darmstadt, Germany

Preprint, December 2011, Department of Mathematics, Technische Universität Darmstadt



TECHNISCHE  
UNIVERSITÄT  
DARMSTADT



**Numerical  
Analysis**



# Model Hierarchy Based Optimal Control of Radiative Heat Transfer

D. Clever

*Department of Mathematics,  
Graduate School of Computational Engineering,  
Technische Universität Darmstadt,  
Dolivostr. 15, D-64293 Darmstadt, Germany  
clever@mathematik.tu-darmstadt.de*

J. Lang

*Department of Mathematics,  
Center of Smart Interfaces, Graduate School of Computational Engineering,  
Technische Universität Darmstadt,  
Dolivostr. 15, D-64293 Darmstadt, Germany  
lang@mathematik.tu-darmstadt.de*

D. Schröder

*Department of Mathematics,  
Technische Universität Darmstadt,  
Dolivostr. 15, D-64293 Darmstadt, Germany  
schroeder@mathematik.tu-darmstadt.de*

December 21, 2011

## Abstract

We present a model hierarchy multilevel optimisation approach to solve an optimal boundary control problem in glass manufacturing. The process is modelled by radiative heat transfer and formulated as an optimal control problem restricted by partial differential algebraic equations (PDAE) and additional control constraints. We consider a sequence of model approximations given by space-time dependent non-linear PDAEs of ascending accuracy. The different models allow for a model hierarchy based optimisation approach, where the models are shifted automatically as the optimisation proceeds. We present a realisation of a multilevel generalised SQP method within the fully space-time adaptive optimisation environment KARDOS using linearly implicit methods of Rosenbrock type and multilevel finite elements. We apply the optimal control algorithm to a glass cooling problem and present numerical experiments for the model hierarchy based approach in two spatial dimensions and for a fully space-time adaptive optimisation in three spatial dimensions.

*Keywords:* optimal boundary control; multilevel; SQP-methods; control constraints; adaptivity; Rosenbrock methods; 3D finite elements; model hierarchy; partial differential algebraic equations; PDAE; radiative heat transfer

## 1 Introduction

During the last decade it has been becoming of growing interest not only to simulate the behaviour of engineering, medical or financial applications but also to optimise their input such that the resulting output follows a desired profile. Usually, the considered process is described by a system of space-time dependent partial differential equations, possibly coupled with algebraic constraints (PDAEs). Mathematically, this results in a so called PDAE-constrained optimal control problem, in general with additional constraints on control and state. For real-world applications, the bottleneck of solving such problems is the high

complexity of the involved PDAEs, which have to be solved several times within each optimisation iteration. Therefore, an efficient optimisation environment has to combine the following two aspects: (i) an optimisation technique with a high order of convergence, such that the number of PDAE solves is brought to a moderate level, and (ii) a fully space-time adaptive PDAE solver of high order, such that the involved PDAEs are solved as efficiently as possible. To even gain more efficiency without loss of accuracy for the optimal control, multilevel techniques are an attractive means.

In this work we present an optimal boundary control problem for the cooling process of hot and already formed glass, which is an important task in glass manufacturing. The cooling process is steered within a furnace, such that the furnace temperature acts on the glass surface only. The task is now to choose a furnace temperature profile that enforces a certain glass temperature evolution, to promote chemical reactions and minimise internal stresses, both at moderate cost. Furthermore, the furnace temperature has to be restricted to a feasible set due to the operation interval of the oven. Because of the high temperatures that occur especially at the beginning of the cooling process, the direction- and frequency-dependent thermal radiation field and the spectral radiative properties of semi-transparent glass play a dominant role. In Section 2, we introduce a seven-dimensional radiative heat transfer model that describes the evolution of the glass temperature and the radiative field depending on the furnace temperature. Since this model is quite expensive, especially for optimisation purposes, we derive suitable approximations, using simplified spherical harmonics and a practically relevant frequency bands model (Farina et al., 2010; Klar et al., 2005; Larsen et al., 2002; Pinnau and Thömmes, 2004). The different models allow for a model hierarchy based optimisation approach, where the optimisation is started on the cheapest model. While the optimisation proceeds, the models are shifted automatically, such that the optimal control is carried out on the most accurate model at the end.

In Section 3 we formulate the cooling process as a PDAE constraint optimal control problem with control constraints and present a realisation of a multilevel generalised SQP method (Ziems, 2010; Ziems and Ulbrich, 2011) within the fully space-time adaptive optimisation environment KARDOS (Clever et al., 2010, 2012; Erdmann et al., 2002). Control constraints are handled by an appropriate projection. Reduced gradients and actings of the reduced Hessian are computed with the continuous adjoint approach. We follow Rothe's method with adaptive Rosenbrock methods in time and adaptive multilevel finite elements in space. To be able to choose the discretisation scheme in accordance to the structure of the considered PDAE, we explicitly allow for an independent discretisation of state and adjoint systems. The resulting inexactness is controlled by refining grids adaptively in space and time as the optimisation proceeds.

In Section 4 we apply the presented algorithm to a glass cooling problem. Note that the presented environment is not restricted to the solution of glass cooling problems. It is a suitable optimisation tool for arbitrary boundary control problems restricted by space-time dependent PDAEs of similar type and constraints on the control. For more details on the class of PDAEs that can be handled we refer to Erdmann et al. (2002). The Section is divided into two subsections. In Subsection 4.1 we solve the optimal control problem for the highest model using the model hierarchy based approach and compare its performance to a similar optimisation run, carried out on the highest model only. Due to the high complexity of the considered model, and the high computing time in three spatial dimensions, we first approximate the three dimensional computational domain by a two dimensional cross section. In Subsection 4.2, we then consider the entire domain and solve the optimal control problem in three space dimensions, considering the less complex grey scale model.

## 2 Glass Cooling

One important step in glass manufacturing is the cooling of the hot and already formed glass down to room temperature. Because the quality of the final product depends highly on the temperature evolution within the glass during the cooling process, there is the need to control the behaviour of the glass temperature. To this end, the hot glass is cooled within a furnace, which is preheated in the beginning. Choosing an optimal course for the temperature reduction within the oven, the temperature evolution within the glass can be influenced in such a way that the resulting product is of high quality.

To be able to compute such an optimal boundary control, it is necessary to derive a suitable model of the cooling process. Because of the high temperatures that occur especially at the beginning of the cooling process, the direction- and frequency-dependent thermal radiation field and the spectral radiative properties of semi-transparent glass play a dominant role. In the following we describe radiation by its intensity  $I(x, t, \nu, s)$ , which depends on the spatial variable  $x \in \Omega \subset \mathbb{R}^d$ ,  $d = 2, 3$ , time  $t \in [0, t_e)$ , frequency  $\nu \in [0, \infty)$ , and direction  $s \in \mathbb{S}^2$  of the unit sphere. Since the prolongation of energy caused by radiation is significantly faster than the one caused by diffusion, it is reasonable to model radiation in a

quasi-static manner. The furnace temperature, denoted by  $u(t)$ , is assumed to be constant in space. Note that, based on the physical background, it occurs only in the boundary conditions. The prolongation of the glass temperature  $T(x, t)$  is modelled by the heat equation and the non-linear exchange of energy between radiation field and glass temperature  $T(x, t)$ . We write the model in a dimensionless form, such that the involved quantities are arranged more clearly. Multiplication with appropriate reference values brings the dimensionless quantities back to its physical counterparts (see e.g. Klar et al. (2005)). The equations read as follows:

$$\epsilon^2 \partial_t T - \epsilon^2 \nabla \cdot (k_c \nabla T) = - \int_{\nu_0}^{\infty} \int_{\mathbb{S}^2} \kappa_\nu (B(T, \nu) - I(x, t, \nu, s)) ds d\nu, \quad (1)$$

$$\epsilon s \cdot \nabla I(x, t, \nu, s) + (\sigma_\nu + \kappa_\nu) I(x, t, \nu, s) = \frac{\sigma_\nu}{4\pi} \int_{\mathbb{S}^2} I(x, t, \nu, s) ds + \kappa_\nu B(T, \nu), \quad \forall \nu > \nu_0, \quad (2)$$

with boundary and initial conditions

$$\epsilon k_c n \cdot \nabla T = h_c (u - T) + \alpha \pi \left( \frac{n_a}{n_g} \right)^2 \int_0^{\nu_0} (B(u, \nu) - B(T, \nu)) d\nu, \quad (3)$$

$$I(x, t, \nu, s) = r(n \cdot s) I(x, t, \nu, s') + (1 - r(n \cdot s)) B(u, \nu), \quad \forall (x, s) \in \partial\Omega \times \mathbb{S}^2 : n(x) \cdot s < 0, \quad (4)$$

$$T(x, 0) = T_0(x). \quad (5)$$

The non-linear exchange of energy between radiative field and the glass itself is described by the scaled Planck function

$$B(T, \nu) = \frac{n_g^2}{c_0^2} \frac{2h_p \nu^3}{I_{\text{ref}} (e^{h_p \nu / (k_b T \cdot T_{\text{ref}})} - 1)}, \quad (6)$$

with Planck constant  $h_p = 6.626e-34 Js$ , Boltzmann constant  $k_b = 1.381e-23 \frac{J}{K}$ , the speed of light in vacuum  $c_0 = 2.998e + 8 \frac{m}{s}$ , and the reference quantities for the glass temperature  $T_{\text{ref}}$  and the intensity  $I_{\text{ref}}$ , respectively. Generally, we set  $T_{\text{ref}} = 1K$  and  $I_{\text{ref}} = 1 \frac{W}{m^2}$ , such that the values of the dimensionless quantities coincide with their dimension-assigned counterpart. For more details concerning the dimensionless model, we e.g. refer to Farina et al. (2010); Larsen et al. (2002).

The definition of the remaining dimensionless parameters is given in Table 1. The concrete values that are used in the numerical experiments are listed in Table 3.

Table 1: Dimensionless parameters of radiative heat transfer model

$\epsilon$	optical thickness coefficient, with $0 < \epsilon \leq 1$ for an optically thick, diffusive regime
$k_c$	heat conduction coefficient
$h_c$	convective heat transfer coefficient
$\kappa_\nu$	frequency-dependent absorption coefficient
$\sigma_\nu$	frequency-dependent scattering coefficient
$n_g$	refractive index: ratio of the speed of light in vacuum and in glass
$n_a$	refractive index: ratio of the speed of light in vacuum and in air
$\nu_0$	upper bound of the opaque spectral region $[0, \nu_0]$
$\alpha$	mean hemispheric surface emissivity in the opaque spectral region
$r$	reflectivity coefficient, with $r \in [0, 1]$
$n(x)$	outwards normal on glass surface

The challenge in solving system (1)-(5) lies in

- the differential algebraic structure, caused by the different time scales of radiation and diffusion,
- the highly non-linear coupling of the glass temperature with the radiative field,
- the six or even seven dimensional phase space.

The high dimension of the phase space makes the numerical solution of the full radiative heat transfer equation (1)-(5) very expensive, which is especially demanding for optimisation purposes, where the system has to be solved several times. Various approximate models that are less time consuming, yet sufficiently accurate, have been developed (Klar et al., 2005; Larsen et al., 2002).

## 2.1 The Models

In the following, we use a first order approximation of simplified spherical harmonics (SP<sub>1</sub>), including a practically relevant frequency bands model. The main idea of this approach is to substitute the direction dependent radiative intensity by an integral mean using asymptotic and variational analysis. In a second step, the continuous frequency spectrum is discretised into  $N$  bands, assuming constant coefficients on each of these bands. The considered SP<sub>1</sub>-approximations have been tested fairly extensively for various radiation transfer problems in glass and have proven to be an efficient way to improve the classical diffusion approximations (Klar et al., 2005; Larsen et al., 2002). By varying the number  $N$  of frequency bands, we derive three different models of rising complexity and accuracy.

**The Augmented Rosseland Approximation.** In its classical form, the Rosseland approximation, which can be also interpreted as an SP<sub>0</sub> approximation, lacks in a proper description of boundary layer effects. Considering the SP<sub>1</sub> approximation of (1)-(5) and replacing the equation of transfer by a pure algebraic equation lead to a significant improvement of the Rosseland approximation, where the boundary conditions are augmented by a radiative term.

The augmented Rosseland approximation results in a space-time dependent partial differential equation of mixed parabolic-elliptic type in one component with state  $y := T$ , given by

$$\partial_t T - \nabla \cdot ((k_c + k_r(T))\nabla T) = 0, \quad (7)$$

equipped with boundary and initial conditions

$$\begin{aligned} n \cdot (k_c + k_r(T))\nabla T &= \frac{h_c}{\epsilon}(u - T) + \frac{\alpha\pi}{\epsilon} \left(\frac{n_a}{n_g}\right)^2 \int_0^{\nu_0} (B(u, \nu) - B(T, \nu))d\nu \\ &+ \frac{4\pi a_1}{\epsilon} \int_{\nu_0}^{\infty} (B(u, \nu) - B(T, \nu))d\nu, \end{aligned} \quad (8)$$

$$T(x, 0) = T_0(x), \quad (9)$$

the boundary condition coefficient  $a_1 = 1.149e-1$  and the thermal conductivity

$$k_r(T) = \frac{4\pi}{3} \int_{\nu_0}^{\infty} \frac{1}{\sigma + \kappa} \partial_T B(T, \nu) d\nu,$$

which is caused by radiation. To evaluate  $k_r$ , we divide the continuous frequency spectrum into eight bands with piecewise constant absorption coefficients  $\kappa_i$ ,  $i = 1, \dots, 8$ , (see Table 2). Furthermore, we set  $\sigma = 0$  for clean glass.

**The Grey Scale Model.** Considering the SP<sub>1</sub> approximation of (1)-(5) and discretising the continuous frequency spectrum by just one single band, we achieve the so called grey scale model. Its name is based on the fact, that in this model we entirely neglect the dependency on wavelength or frequency. It is given by the following space-time dependent partial differential algebraic equations of mixed parabolic-elliptic type in two components with state  $y := (T, \phi)^T$ :

$$\partial_t T - k_c \Delta T - \frac{1}{3(\kappa + \sigma)} \Delta \phi = 0 \quad (10)$$

$$-\frac{\epsilon^2}{3(\kappa + \sigma)} \Delta \phi = -\kappa \phi + 4\pi \kappa a_2 T^4 \quad (11)$$

with boundary and initial conditions

$$k_c n \cdot \nabla T + \frac{1}{3(\kappa + \sigma)} n \cdot \nabla \phi = \frac{h}{\epsilon}(u - T) + \frac{1}{2\epsilon} (4\pi a_2 u^4 - \phi) \quad (12)$$

$$\frac{\epsilon^2}{3(\kappa + \sigma)} n \cdot \nabla \phi = \frac{\epsilon}{2} (4\pi a_2 u^4 - \phi) \quad (13)$$

$$T(0, x) = T_0(x), \quad (14)$$

and the radiated energy coefficient  $a_2 = 1.8e-8$ .

**The Eight Band Model.** We again consider the  $SP_1$  approximation of (1)-(5), but now we discretise the continuous frequency spectrum into eight bands  $[\nu_{i-1}, \nu_i]$ ,  $i = 0, \dots, 8$ , where we formally set  $\nu_8 := \infty$  and  $\nu_{-1} := 0$ , see Figure 1. On each of the bands we interpret frequency dependent quantities as constants. The values are given in Table 2. Defining the frequency-independent mean of the Planck function

$$B^{(i)}(\nu) := \int_{\nu_{i-1}}^{\nu_i} B(\nu, \nu) d\nu, \quad i = 1, \dots, 8, \quad (15)$$

the eight band model is given by the following system of space-time dependent partial differential algebraic equations of mixed parabolic-elliptic type in nine components with state  $y := (T, \phi_1, \dots, \phi_8)^T$ :

$$\partial_t T - \nabla \cdot (k_c \nabla T) = \sum_{i=1}^8 \nabla \cdot \left( \frac{1}{3(\sigma_i + \kappa_i)} \nabla \phi_i \right), \quad (16)$$

$$-\epsilon^2 \nabla \cdot \left( \frac{1}{3(\sigma_i + \kappa_i)} \nabla \phi_i \right) + \kappa_i \phi_i = 4\pi \kappa_i B^{(i)}(T), \quad i = 1, \dots, 8, \quad (17)$$

with boundary and initial conditions

$$k_c n \cdot \nabla T + \sum_{i=1}^8 \frac{1}{3(\sigma_i + \kappa_i)} n \cdot \nabla \phi_i = \frac{h_c}{\epsilon} (u - T) + \frac{\alpha \pi}{\epsilon} \left( \frac{n_a}{n_g} \right)^2 \left( B^{(0)}(u) - B^{(0)}(T) \right) + \frac{a_1}{\epsilon} \sum_{i=1}^8 \left( 4\pi B^{(i)}(u) - \phi_i \right), \quad (18)$$

$$\frac{\epsilon^2}{3(\sigma_i + \kappa_i)} n \cdot \nabla \phi_i = a_1 \epsilon \left( 4\pi B^{(i)}(u) - \phi_i \right), \quad i = 1, \dots, 8, \quad (19)$$

$$T(x, 0) = T_0(x), \quad (20)$$

and the boundary condition coefficient  $a_1 = 1.149e-1$ .

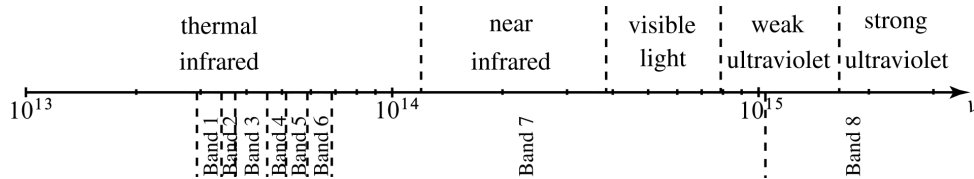


Figure 1: The continuous frequency spectrum is approximated by a discrete eight-band model with constant coefficients on each interval.

Table 2: Absorption coefficients of eight band model

Band $i$	$\nu_{i-1} (10^{13} s^{-1})$	$\nu_i (10^{13} s^{-1})$	$\kappa_i (m^{-1})$
-	0	2.9334638	opaque
1	2.9334638	3.4223744	7136.00
2	3.4223744	3.7334994	576.32
3	3.7334994	4.5631659	276.98
4	4.5631659	5.1335616	27.98
5	5.1335616	5.8669276	15.45
6	5.8669276	6.8447489	7.70
7	6.8447488	102.6712329	0.50
8	102.6712329	$\infty$	0.40

## 2.2 Model Hierarchy

With the three models described above, we have a sequence of approximations to the full radiative heat transfer model with ascending accuracy and complexity. To determine an optimal furnace temperature

evolution for a real cooling process, it is clearly desirable to consider the most accurate model. However, from an efficiency point of view the lowest model is the natural candidate of choice, especially for optimisation purposes. To serve both accuracy and efficiency, we consider the optimal control problem on a model hierarchy, where most of the optimisation iterations are carried out on cheap models but where at least the last iteration, and hence the optimal control, is computed using the best model available.

Let a sequence of models  $M_i$ ,  $i = 1, \dots, m$ , with ascending accuracy be given. We take for  $M_1$  the Rosseland approximation, for  $M_2$  the grey scale, and for  $M_3$  the eight band model. Furthermore, we define some criticality measure  $C_M$ , which decreases while the control iterates approach the optimal control. We now shift from the current model  $M_i$  to the next higher order model  $M_{i+1}$  if an appropriate error estimate  $E(M_i, M_{i+1})$  exceeds the scaled criticality measure, i.e.,

$$\begin{aligned} &\text{shift from model } M_i \text{ to model } M_{i+1}, \text{ if} \\ &E(M_i, M_{i+1}) > k_i C_M. \end{aligned} \quad (21)$$

For the glass cooling problem, it is reasonable to estimate the error between the different models by considering the difference in the glass temperature over space and time. Note that neither the mean intensities nor the entire state are a meaningful candidate, since they differ in the three models. For  $T : \Omega \times [0, t_e] \rightarrow \mathbb{R}$ , we define

$$E(M_i, M_{i+1}) := \|T_{M_i} - T_{M_{i+1}}\|_{L^2(\Omega \times [0, t_e])} = \left( \int_0^{t_e} \int_{\Omega} (T_{M_i}(x, t) - T_{M_{i+1}}(x, t))^2 dx dt \right)^{\frac{1}{2}}, \quad (22)$$

which can be evaluated with nearly no extra effort, see Subsection 3.3. An implementation of a model hierarchy based SQP method and a comparison to the corresponding realisation on the highest order model is presented and discussed in Section 4.

### 3 Optimisation Environment

To determine a furnace temperature profile that enforces an efficient cooling while maintaining a high quality of the manufactured glass we interpret the setting as an optimal boundary control problem. To this end we define an objective functional that measures the quality of the furnace temperature profile and the resulting temperature evolution within the glass. The optimal control is computed by minimising this objective with respect to the considered glass cooling model and with upper and lower bounds for the furnace temperature.

For the optimisation, we consider derivative based optimisation algorithms and follow the so called continuous adjoint approach. More details on the optimal control problem and the determination of the derivatives are given in Subsection 3.1. In Subsection 3.2 we introduce a multilevel generalised SQP method (Clever et al., 2010, 2012; Ziems, 2010; Ziems and Ulbrich, 2011), which allows for point-wise constraints on the control. Its coupling with the state-of-the-art PDAE solver KARDOS is presented in Subsection 3.3.

#### 3.1 Optimal Control Problem

To determine an appropriate optimal control, it is essential to formulate a sound objective. In the context of glass cooling we deal with at least two contrary criteria. An important aim is to force the glass temperature function as close as possible to a desired temperature profile. Such a profile, for which good performance of the involved chemical processes is known, is generally given by engineers. A common approach is to choose the tracking function for the glass temperature spatially constant in order to enforce a homogeneous cooling with small temperature gradients. This is necessary to reduce internal stresses and avoid cracks within the glass. Note that, because the cooling is controlled at the boundary only, such a guiding function can only be approached but not necessarily reached within the entire domain. Furthermore, it is desirable to pay certain attention to the glass temperature at the final time, which is realised by an additional term in the objective. Especially in the context of the continuous adjoint calculus, such a term is of great importance, since it affects the initial values of the adjoint systems (Clever and Lang, 2011). Finally, the objective has to include a regularisation of the control itself. This term can be used to search an optimal control close to a preferable profile or to minimise the manufacturing costs. An objective functional that meets all the requirements stated above can be defined by

$$J(T, u) := \frac{1}{2} \int_0^{t_e} \|T - T_d\|_{L^2(\Omega)}^2 dt + \frac{\delta_e}{2} \|(T - T_d)(t_e)\|_{L^2(\Omega)}^2 + \frac{\delta_u}{2} \int_0^{t_e} (u - u_d)^2 dt, \quad (23)$$

with the desired glass temperature distribution  $T_d(x, t)$ , the guideline for the control  $u_d(t)$  and the Tikhonov parameters  $\delta_u$  and  $\delta_e$ . For more complex objective functionals within the context of glass cooling, including time dependent weights and a term forcing the minimisation of internal stresses explicitly, we refer to Clever and Lang (2011). Additionally, it is important to restrict the control  $u$  to a convex, feasible set  $U_{ad}$ , which represents the operation interval of the furnace.

In the following, let the state system of the optimal control problem be denoted by

$$e(y, u) = 0. \quad (24)$$

Depending on the model chosen, the state system is defined by one of the approximations (7)-(9), (10)-(14) or (16)-(20), respectively. Assuming  $J(y, u)$  and  $e(y, u)$  to be twice continuously Fréchet differentiable, which is obvious for the objective (23) and was shown for the grey scale model in Pinnau (2007), it is a common approach to reduce the optimisation problem to its control component, such that the reduced optimal control problem reads

$$\min_{u \in U_{ad}} \hat{J}(u) := J(y(u), u), \quad \text{where } y = y(u) \text{ satisfies } e(y, u) = 0. \quad (25)$$

The feasible subset  $U_{ad}$  of the control space  $U$  is defined by

$$U_{ad} := \{u \in U : u_{low} \leq u(t) \leq u_{up}, \forall t \in [0, t_e]\}, \quad (26)$$

with upper bound  $u_{up}$  and lower bound  $u_{low}$ . Denoting the adjoint operator of the state operator by  $e^*(y, u)$ , the reduced gradient is given by

$$\nabla \hat{J}(u) = \nabla_u J(y, u) + \nabla_u e^*(y, u)\xi, \quad (27)$$

where  $\xi$  is the adjoint state, which can be computed by solving the adjoint system

$$\partial_y J(y, u) + \partial_y e^*(y, u)\xi = 0. \quad (28)$$

A formal description of this process is shown in Figure 2.

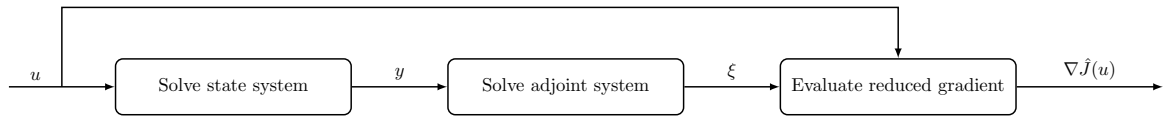


Figure 2: Computation of reduced gradient by adjoint calculus

Instead of the whole reduced Hessian  $\hat{J}''(u)$ , we only consider actings of it, that can efficiently be computed by evaluating

$$\hat{J}''(u)s_u = \partial_{uu}J(y, u)s_u + \partial_{uu}e^*(y, u)\xi s_u + \partial_u e^*(y, u)w + \partial_{uy}J(y, u)s_y + \partial_{uy}e^*(y, u)\xi s_y, \quad (29)$$

with some direction  $s_u$ , the linearised state  $s_y$ , and the second adjoint state  $w$ . The linearised state  $s_y$  is the solution of the linearised state system

$$\partial_y e(y, u)s_y = -\partial_u e(y, u)s_u, \quad (30)$$

with input  $s_u$ , and the second adjoint state is the solution of the second adjoint system

$$\partial_y e^*(y, u)w = -\partial_{yy}J(y, u)s_y - \partial_{yy}e^*(y, u)\xi s_y - \partial_{yu}J(y, u)s_u - \partial_{yu}e^*(y, u)\xi s_u, \quad (31)$$

which depends on state  $y$ , linearised state  $s_y$  and adjoint state  $\xi$ . The complete data flow is illustrated in Figure 3. Note that it is inefficient to compute all components of the reduced Hessian, since this would require at least  $2m$  additional PDAE solves, where  $m$  is the number of discretisation points of the control space. Contrarily, the adjoint based approach presented above requires only two additional PDAE solves, independent of the discrete control space.

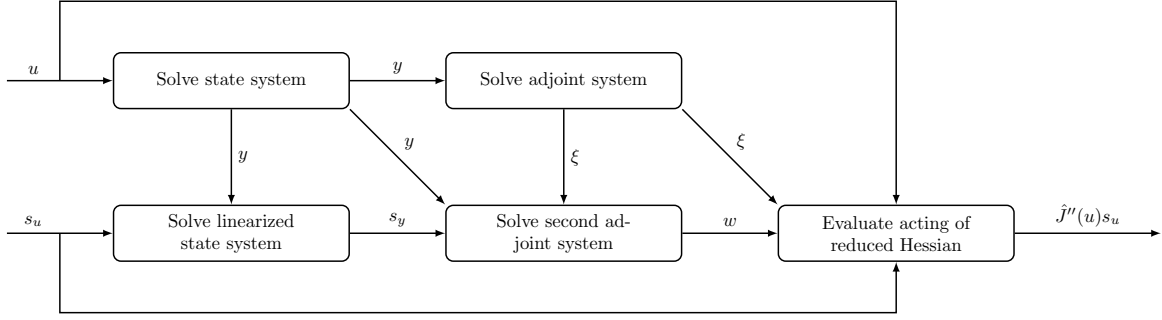


Figure 3: Computation of acting of reduced Hessian by adjoint calculus

### 3.2 Multilevel Generalised SQP Method

In the following, we consider a multilevel generalised SQP method that explicitly allows the use of independent discretisation schemes and independent spatial meshes for state and adjoint equations, see Clever et al. (2010, 2012); Ziems (2010); Ziems and Ulbrich (2011). Enriched with a fully space time adaptive PDAE solver, this has the advantage that we can perfectly exploit the structure of each PDAE independently from the other involved PDAEs, gaining a high degree of efficiency. Clearly, allowing for independent discretisations for state and adjoint equations introduces inconsistencies between reduced derivatives and the minimisation problem itself. Therefore, the algorithm is enriched by a multilevel strategy that tailors the grid refinement in accordance to the optimisation progress.

The main idea of the SQP method is to approximate the reduced optimisation problem (25) by a sequence of reduced SQP-subproblems:

$$\min_{s_u \in U_{ad} - u_k} \hat{q}_k(s_u) := J(y_k, u_k) + \langle \hat{J}'(u_k), s_u \rangle + \frac{1}{2} \langle s_u, \hat{J}''(u_k) s_u \rangle \quad \text{s.t. } \|s_u\| \leq \Delta_k, \quad (32)$$

with reduced gradient  $\hat{J}'(u_k)$ , reduced Hessian  $\hat{J}''(u_k)$  and trust region radius  $\Delta_k$ . When solving (32) we have to account for four characteristics. The first two points are, that the search direction  $s_u$  is restricted to the set  $U_{ad} - u_k$  and its length to the trust region radius  $\Delta_k$ . The third point is, that we only need actings of the reduced Hessian  $\hat{J}''(u_k) s_u$  and the last, that the reduced Hessian is not necessarily symmetric due to the different discretisation schemes in state and adjoint systems and the independent spatial meshes. To handle the control constraints, we define the  $\varepsilon$ -active set

$$\mathcal{A}^\varepsilon(u_k^h) = \{i | (u_{\text{up}}^h)_i - (u_k^h)_i \leq \varepsilon \text{ or } ((u_k^h)_i - u_{\text{low}}^h)_i \leq \varepsilon\}, \quad (33)$$

where  $(u^h)_i$  denotes the  $i$ -th component of the discretised control  $u^h$ . The  $\varepsilon$ -inactive index set  $\mathcal{I}^\varepsilon(u_k^h)$  is defined by the complement  $\mathcal{A}^\varepsilon(u_k^h)^c$ . Here and in the following we set  $\varepsilon = \min\{C_M, (u_{\text{up}} - u_{\text{low}})/2\}$ , with criticality measure  $C_M$ , upper bound  $u_{\text{up}}$  and lower bound  $u_{\text{low}}$ , to avoid an overlapping of active regions. Because we only have actings of the slightly unsymmetrical Hessian, we consider a restricted version of BiCGstab, which solves the linear equation

$$\hat{J}''(u_k) s_u = -\nabla \hat{J}(u_k) \quad (34)$$

only on the  $\varepsilon$ -inactive part, delivering the solution  $s_u^{\mathcal{I}^\varepsilon(u_k)}$ . In the  $\varepsilon$ -active region, a projected gradient step  $s_u^{\mathcal{A}^\varepsilon(u_k)} := -\nabla \hat{J}(u_k)|_{\mathcal{A}^\varepsilon(u_k)}$  is considered. Using Armijo's line search, a proper scaling  $\sigma_k$  of the trial step

$$s_{u,\text{proj}} := P_{U_{ad} - u_k}(\sigma_k s_u), \text{ with } s_u := s_u^{\mathcal{I}^\varepsilon(u_k)} + s_u^{\mathcal{A}^\varepsilon(u_k)}, \quad (35)$$

is determined. The projection  $P_{U_{ad} - u_k}(d)$  of a quantity  $d$  is defined, such that  $u_k + P_{U_{ad} - u_k}(d)$  is within the feasible set  $U_{ad}$ . A new control  $u_{k+1} := u_k + \sigma s_{u,\text{proj}}$  is accepted, if the actual reduction

$$\text{ared}_k = J(y_k, u_k) - J(y_{k+1}, u_{k+1}) \quad (36)$$

is at least a fraction of the model based predicted reduction

$$\text{pred}_k = \hat{q}_k(0) - \hat{q}_k(s_{u,\text{proj}}). \quad (37)$$

If a step is accepted, the ratio of actual and predicted reduction is used in a standard fashion to adjust the trust region radius  $\Delta_k$ . If a step is rejected, it has to be verified, if either the SQP-subproblem (32) does not approximate the optimisation problem (25) well enough or if full and reduced model do not coincide well enough on the current discretisation level. In the first case, the trust region gets reduced and in the second, the accuracy level gets increased.

Independently of acceptance or rejection of a new control, for a sufficient quality of space and time grids, we require

$$\eta_y \leq c_1 C_M, \quad (38)$$

$$\eta_\xi \leq c_2 C_M, \quad (39)$$

with criticality measure  $C_M$  and global discretisation error estimators  $\eta_y$  and  $\eta_\xi$ , see Subsection 3.3. If the criticality measure descends below a predefined tolerance, the algorithm is stopped. For more details on the algorithm we refer to Clever et al. (2010, 2012); Ziems (2010); Ziems and Ulbrich (2011).

In later computations we define the criticality measure  $C_M$  by the projection of the reduced gradient

$$C_M = \|P_{U_{ad}-u_k}(\hat{J}'(u_k))\|. \quad (40)$$

Note that we use the same criticality measure  $C_M$  to control the model hierarchy in (21). A flow chart that illustrates the performance of the considered multilevel hierarchy based SQP-method is presented in Figure 4.

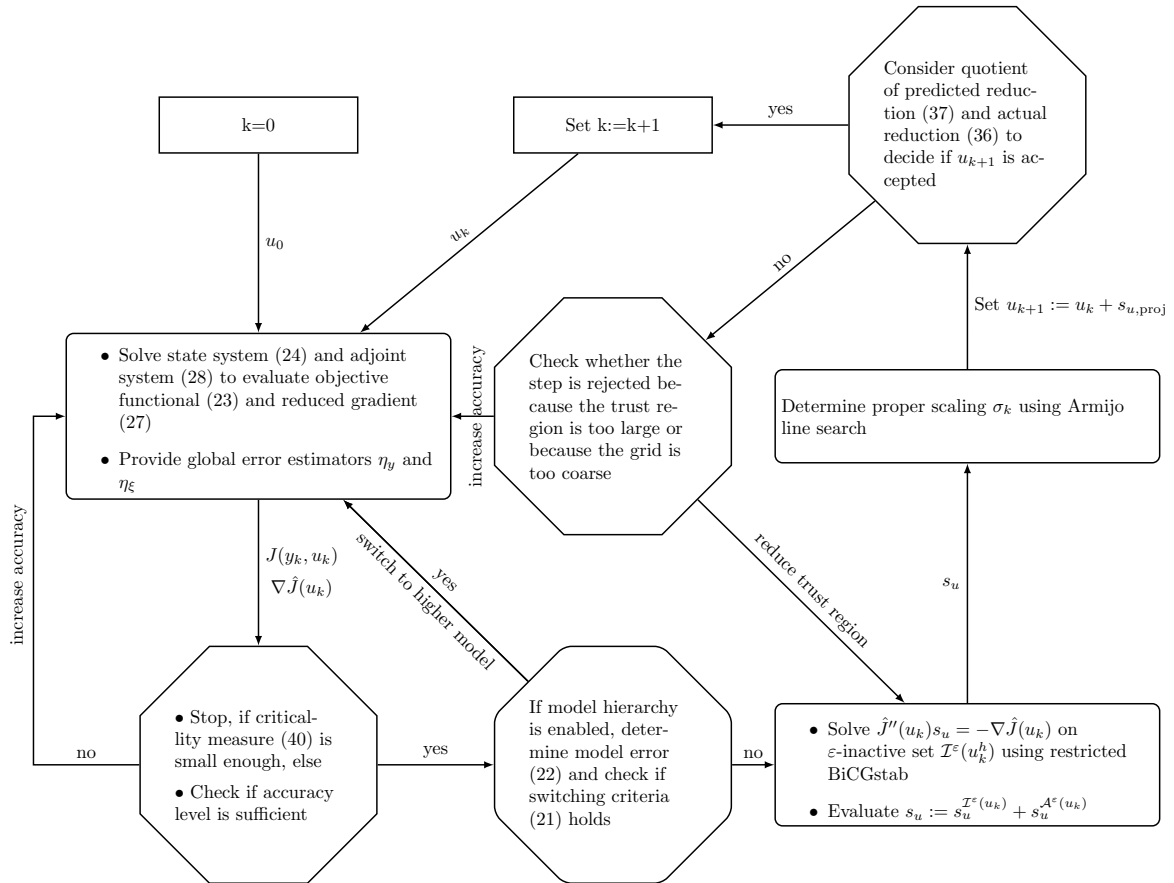


Figure 4: Schematic representation of multilevel hierarchy based SQP-method  
In the flow chart decisions are visualised by octagons, other tasks by rectangles. Rounded corners mark tasks, that include at least one PDAE solve. Note that the BiCGstab box includes the evaluation of actings of the reduced Hessian (29) in every iteration.

### 3.3 Realisation

To solve the involved systems of PDAEs, to evaluate functionals like objective and reduced derivatives and to estimate discretisation errors, we couple the optimisation algorithm with the fully space-time

adaptive software package KARDOS. It is based on Rothe’s method with adaptive linearly implicit one-step method of Rosenbrock type for the time integration and adaptive multilevel finite elements for the spatial discretisation. The linearly implicit structure of the Rosenbrock methods is advantageous to handle non-linearities, like the Planck function in the glass cooling problem. The one-step character allows rapid change of step sizes, which are adjusted with respect to local error estimates determined by an embedded scheme of inferior order. To control the adaptive grid refinement in space, the spatial discretisation error is estimated locally by the hierarchical basis concept (Lang, 2001).

KARDOS offers the possibility to make PDAE solutions from previous runs available to the current PDAE solve. This mechanism can be used to solve state and adjoint systems sequentially, to evaluate the reduced gradient as illustrated in Figure 2 and to evaluate the reduced Hessian, see Figure 3. Figure 5 gives a closer look at the underlying grid and data management in KARDOS. Because state and linearised state equation have initial conditions, those two systems are solved forward in time, whereas adjoint and second adjoint system with their terminal conditions are solved backwards in time. Each of the four systems can be solved with a different integration method that matches the structure of the underlying PDAE. On each accuracy level, an adaptive time discretisation  $t_0, t_1, \dots, t_n$  is determined during the state system solve. This discretisation is reused for all other PDAE solves as long as the resulting global error estimates  $\eta_y$  and  $\eta_\xi$  fulfil (38) and (39). In each point of time  $t_k$ , the Rosenbrock discretisation results in a sequence of elliptic PDEs, which are solved on their own suitable grid. Hence, when setting up adjoint and second adjoint system the environment has to manage the transfer from up to three PDAE solutions, which have been computed on their own independent spatial mesh. The computations are done partly forwards and partly backwards in time. Note that the same mechanism can be used to evaluate the

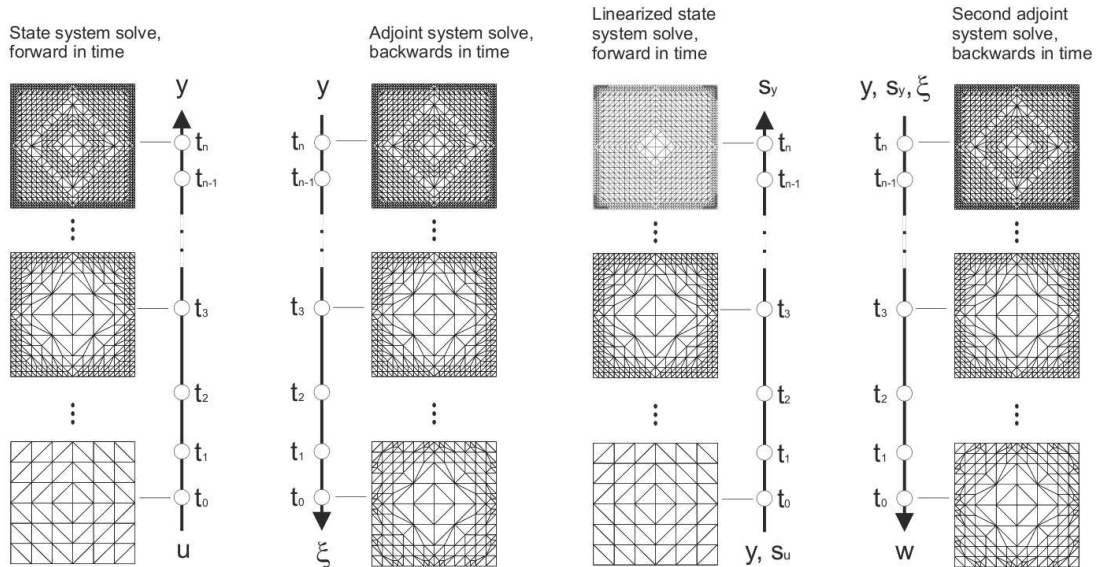


Figure 5: Grid and data management

On each accuracy level, an adaptive time discretisation  $t_0, t_1, \dots, t_n$  is determined during the state system solve, which is then used for all other PDAE solves on this level. In each point of time  $t_k$ , the Rosenbrock discretisation results in a sequence of elliptic PDEs, which are solved on their own suitable spatial grid by finite elements. Solving the adjoint system backwards in time on the predefined time grid, the spatial meshes are individually adapted to reach the desired accuracy. To provide a current PDAE solve with solutions from previous runs, the solution is imported on its computational grid and transferred to the current grid.

model error (22). In this case a lower model solution is read in during a higher model solve. Having both solutions on the same grid, the  $L^2$ -norm of their difference can be efficiently evaluated by a weighted sum. On each accuracy level the procedure is the same as presented in the flow chart 5, but with increasing number of time nodes. This results in an increasing number of elliptic differential equations, each of them solved on a individually refined grid ensuring the new accuracy. To provide global error estimates  $\eta_y$  and  $\eta_\xi$  for the multilevel strategy in (38)-(39), we make use of the already computed local error estimates and rely on tolerance proportionality. With respect to the semi-discretisation, we distinguish between the local error in time  $le^t = (0, le_1^t, \dots, le_n^t)$  and the local error in space  $le^x = (0, le_1^x, \dots, le_n^x)$  and define

the global estimate

$$\eta = (t_e - t_0)^{-\frac{1}{2}} \left( \left( \sum_{k=0}^{n-1} \frac{\tau_k}{2} ((le_k^t)^2 + (le_{k+1}^t)^2) \right)^{1/2} + \left( \sum_{k=0}^{n-1} \frac{\tau_k}{2} ((le_k^x)^2 + (le_{k+1}^x)^2) \right)^{1/2} \right), \quad (41)$$

with adaptive time step sizes  $\tau_k$ ,  $k = 0, \dots, n-1$ .

Considering the local error estimate (41) within the state system (24) evaluates  $\eta_y$ . Using the local error estimate (41) within the adjoint system (28) evaluates  $\eta_\xi$ . The unknown proportionality factors can formally be handled by the constants  $c_1$  and  $c_2$ .

We want to point out, that the KARDOS based multilevel SQP algorithm is not restricted to the solution of the glass cooling problem. It is a suitable optimisation tool for arbitrary boundary control problems restricted by space-time dependent PDAEs of similar type. For more details on the class of PDAEs that can be handled we refer to Erdmann et al. (2002).

## 4 Numerical Experiments

The following Section is divided into two subsections. In Subsection 4.1 we solve the optimal control problem for the eight band model using the model hierarchy based approach, explained in Subsection 2.2. We compare its performance with respect to quality and effort to a similar optimisation run, carried out on the eight band model only. Due to the high complexity of the considered model, and the high computing time in three spatial dimensions, in this subsection we approximate the three dimensional computational domain by a two dimensional cross section. In Subsection 4.2, we then consider the entire domain and solve the optimal control problem in three space dimensions, considering the less complex grey scale model. The computational domain  $\Omega_{3d}$  is given by the convex hull of the eight points

$$\begin{aligned} p_1 &= (-1, -1, -1), & p_2 &= (1, -1, -1), & p_3 &= (1, 1, -1), & p_4 &= (-1, 1, -1), \\ p_5 &= (0.5, 0.5, 1), & p_6 &= (1, 0.5, 1), & p_7 &= (1, 1, 1), & p_8 &= (0.5, 1, 1). \end{aligned}$$

To define a two dimensional cross section we set  $z = \frac{1}{3}$ , which results in  $\Omega_{2d} = [0, 1] \times [0, 1]$ . Both geometries, together with their initial grids, are shown in Figure 6.

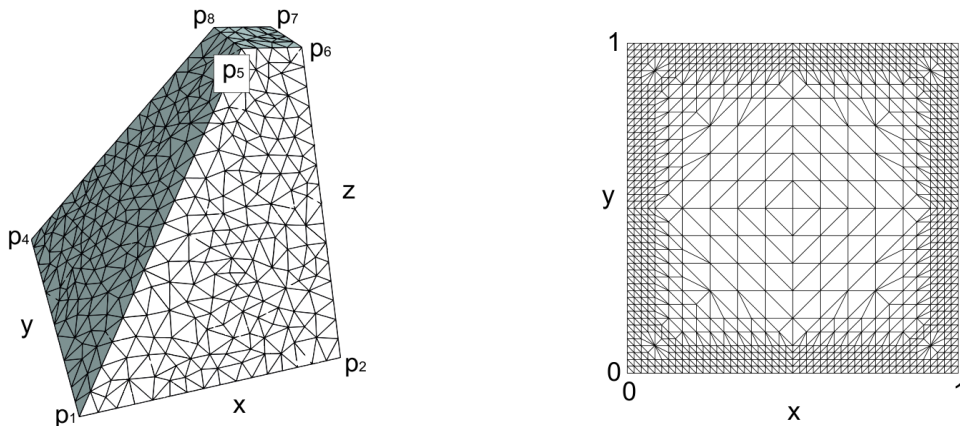


Figure 6: Three dimensional computational domain and two dimensional cross section  $z = \frac{1}{3}$ , with initial grids

Further parameters concerning the different models and the optimisation algorithm are given in Table 3. In the following numerical experiments we use linear finite elements and the third order Rosenbrock method ROS3PL (Lang and Verwer, 2001; Lang and Teleaga, 2008), which is an L-stable time integration scheme and does not suffer from order reduction.

### 4.1 Model Hierarchy Approach

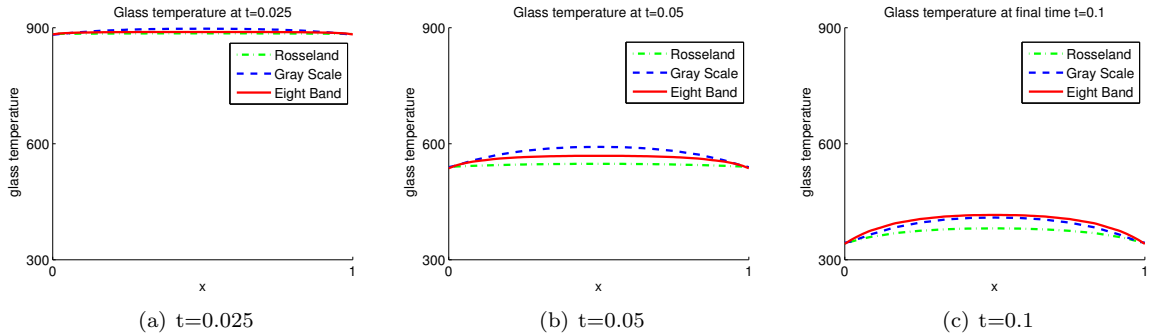
In this section we present the model hierarchy based SQP method presented in Section 3. For the model hierarchy, we consider all three models (7)-(9), (10)-(14) and (16)-(20), which means that we finish the

Table 3: Problem and model specific qualities

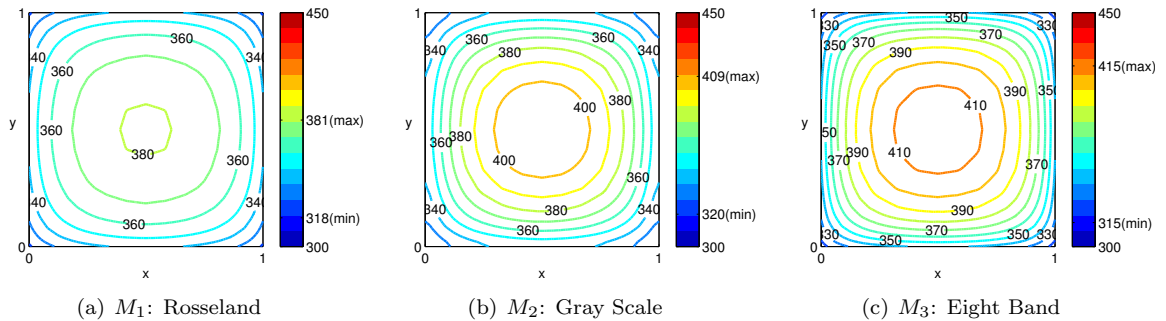
$U_{ad}$	feasible control set	$[300, 900]$	$k_c$	conductivity coefficient	$1.0e+0$
$t_e$	final time	$1.0e-1$	$h_c$	convection coefficient	$1.0e-3$
$T_0(x)$	initial glass temperature	$9.0e+2$	$\epsilon$	optical thickness coeff.	$5.0e-1$
			$\alpha$	mean hemispheric surface emissivity	0.914
$T_d(t)$	desired glass temperature	$T_0 \cdot e^{-\frac{\log(\frac{T_0}{300})t}{t_e}}$	$n_g$	refractive index for glass	$1.46e+0$
$u_0(t)$	initial control	$T_d(t)$	$n_a$	refractive index for air	$1.0e+0$
$u_d(t)$	desired control	$T_d(t)$	$a_1$	boundary condition coefficient	$1.149e-1$
$\delta_e$	final value weight	$1.0e-1$	$a_2$	radiated energy coefficient	$1.8e-8$
$\delta_u$	control regularisation weight	$1.0e-1$	$h_p$	Planck constant	$6.626e-34 Js$
$\Delta_k$	trust region	$5.0e+2$	$k_b$	Boltzmann constant	$1.381e-23 \frac{J}{K}$
			$c_0$	speed of light in vacuum	$2.998e+8 \frac{m}{s}$

algorithm with an optimal control for the eight band model. As an approximative weighted mean of the absorption rates of the different bands, given in Table 2, the mean absorption coefficient  $\kappa$  in the grey scale problem is set to  $\kappa = 10$ . The results of the hierarchy based approach are compared to those that result from a similar optimisation carried out on the eight band model only. Due to the quite high complexity of this one-model approach, we first replace the three dimensional computational domain by the two dimensional cross section  $\Omega_{2d} = [0, 1] \times [0, 1]$ , see Figure 6. Furthermore, we carry out all PDAE solves on a predefined space-time grid, which is refined in the boundary region, with 76 time steps and 1053 spatial nodes. The mesh is chosen in such a way, that there is no further refinement necessary during the entire optimisation. Note that this simplification is only made to be able to study the benefit of the model hierarchy. Full space-time adaptivity and a grid refining multilevel strategy as explained in Section 3 are considered in Subsection 4.2 for three space dimensions. For an application to the glass cooling problem in two space dimensions, we refer to Clever et al. (2010, 2012).

The constants  $k_1$  and  $k_2$  that steer the shifting from one model to another, see (21), are set to  $k_1 = k_2 = 1.0$ . To get an impression about the similarity of the three models, Figure 7 shows the glass temperature on the cut section through  $y = 0.5$  at different points of time for all three models, resulting from the initial control  $u_0$ . The corresponding temperature distribution over the entire domain

Figure 7: Glass temperature on cut section through  $y = 0.5$  at different points of time

$[0, 1] \times [0, 1] \in \mathbb{R}^2$  for the final time is shown in Figure 8. For a better visualisation of the temperature

Figure 8: Glass temperature distribution at final time for the models  $M_1$ ,  $M_2$  and  $M_3$

differences, the colour is scaled between 300 and 450, which is the lower quarter of the feasible set  $U_{ad}$ . The computations were carried out on a AMD Athlon(tm) 64 X2 Dual Core Processor 6000+, with a CPU cache size of 512 KB and a clock rate of 1000 MHz. On the predefined grid the state system solve of the Rosseland approximation requires 26s, that of the grey scale model 49s, and that of the eight band model 400s. We clearly see a ratio of 1 : 2 : 16. Due to the nearly linear scaling of the KARDOS code with respect to the degrees of freedom, these factors are also valid for arbitrary space-time resolutions.

We now start the algorithm for the Rosseland model  $M_1$  with initial control  $u_0$ . After two optimisation iterations the model error  $E(M_1, M_2)$  exceeds the criticality measure  $C_M$  and hence the model is shifted automatically to the grey scale model  $M_2$ . After two optimisation iterations on this level, the model error  $E(M_2, M_3)$  exceeds the criticality measure  $C_M$  again, and the model is finally shifted to the eight band model  $M_3$ . After every model change the criticality measure increases, which shows that an almost optimal control for one model is not necessarily optimal for another model. However, it is a good approximation of it and can be interpreted as an efficiently computed initial control. We stop the algorithm if the criticality measure falls below the limit of  $5.0e-4$  and refer to the last control iterate as optimal control. This optimal control together with the initial control is presented in Figure 9(a). The evolution of the glass temperature over time that results from the optimal control is shown in Figure 9(b) for the boundary point  $Q_1 = (0, 0.5)$ , the corner point  $Q_2 = (1, 0)$ , and the interior point  $Q_3 = (0.5, 0.25)$ . Note that the

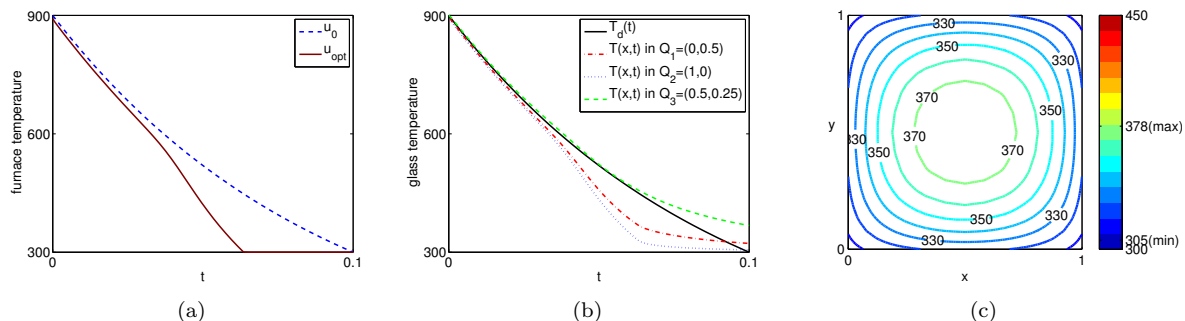


Figure 9: Initial and optimal control and resulting glass temperature evolution

Figure 9(a) shows the initial and the optimal control determined by the model hierarchy based approach, Figure 9(b) the evolution of the glass temperature resulting from the optimal control over time in a boundary point  $Q_1$ , a corner point  $Q_2$  and an interior point  $Q_3$ , and Figure 9(c) the glass temperature distribution over the entire domain at final time.

glass temperature within the computational domain is mainly located between the temperature of the boundary point  $Q_1$  (green dashed line) and the interior point  $Q_3$  (red dot-dashed line), see 9(b). Hence, the optimal glass temperature is evenly distributed around the desired profile  $T_d(t)$ . Contrarily, for the initial control, the resulting glass temperature distribution lies above  $T_d(t)$  in any space-time point of the computational domain. The glass temperature distribution over the entire domain at final time, resulting from the optimal control, is shown in Figure 9(c). Comparing it to the distribution resulting from the initial control, see Figure 8(c), we can observe a significant improvement. More details about the optimisation performance are given in Table 4.

Comparing the model hierarchy based approach to a similar optimisation that is already started with the eight band model, see Table 5, it can be observed, that now the algorithm determines an optimal control of comparable accuracy in  $k = 5$  instead of  $k = 7$  optimisation iterations. However, the model hierarchy based approach needs only 3 optimisation iterations on the time consuming eight band model, see Table 4. It is necessary to additionally compute the model error for the two lower models. However the effort for the optimisation iterations on these models is almost negligible in comparison to the complexity of the eight band model. Having a look at the computing time (Table 4 and Table 5), it can be seen that the model hierarchy based approach saves about 20% of the computational time required by the one-model approach.

Studying the results of the two algorithms, we clearly observe a significant different development of the control iterates in each optimisation step, see Figure 10. But, as expected, the optimal controls that result from the two approaches are nearly identical. Their relative  $L^2$ -difference is  $1.578e - 06$ . Due to the great conformance of the optimal control from both approaches, we abstain from showing further results for the one-model approach, since they coincide with those presented for the model hierarchy based approach in Figure 9.

Summarising, it can be said that for a reasonable hierarchy of different models with ascending accuracy,

Table 4: Optimisation protocol for the model hierarchy based approach

opt. iter.	target value	criticality measure	model error $E(M_i, M_{i+1})$	time to compute $E$ [s]	#BiCGstab iterations	accumulated CPU time [s]
Start with Rosseland approximation						
	2.4213889e+02	1.320e+01	2.804e-01	45		139
1	8.9556646e+01	6.420e-01	3.143e-01	45	5	1 192
2	8.9018226e+01	6.828e-02	3.143e-01	44	4	2 097
Shift to grey scale model						
	1.5892804e+02	6.010e+00	1.504e-01	392		2 570
3	1.3618194e+02	3.657e-01	1.575e-01	391	4	3 377
4	1.3605275e+02	7.212e-03	1.579e-01	391	3	4 432
Shift to eight band model						
	1.9479777e+02	2.230e+00	-	-		5 575
5	1.9113854e+02	1.126e-01	-	-	4	14 647
6	1.9112199e+02	2.544e-03	-	-	3	21 995
7	1.9112197e+02	2.367e-04	-	-	1	25 853

Table 5: Optimisation protocol for the eight band model

optimisation iteration	target value	criticality measure	#BiCGstab iterations	accumulated CPU time [s]
	4.5934272e+02	1.835e+01		1 268
1	1.9478452e+02	1.763e+00	4	10 387
2	1.9118843e+02	2.163e-01	3	17 716
3	1.9112234e+02	7.690e-03	3	25 043
4	1.9112200e+02	7.283e-04	1	28 831
5	1.9112198e+02	1.576e-04	1	32 625

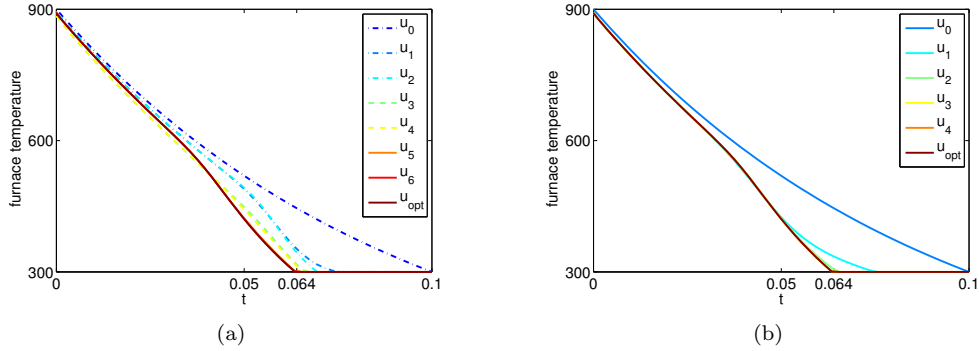


Figure 10: Comparison between model hierarchy and eight band model

Control iterates determined by model hierarchy based approach 10(a) and determined entirely on eight band model 10(b). Iterates computed with the Rosseland approximation are plotted with a dot-dashed line, those of the grey scale model with a dashed line, and those of the eight band model with a solid line. Even though the model hierarchy based approach requires two additional optimisation iterations it determines the same optimal control significantly faster than the one-model optimisation.

the presented model hierarchy based approach is a suitable tool to decrease the computational effort while maintaining the desired accuracy. As long as the optimisation is entirely carried out on the same level of accuracy we observe savings in the computing time of around 20%. However, when the grid refining multilevel strategy, presented in Section 3, is enabled as well, the last optimisation iteration might require more than 90% of the entire computing time. To serve the desired accuracy, this expensive step has to be carried out in the model hierarchy based approach as well. Hence in such a case, a benefit of 20% from the remaining 10% does only result in a benefit of 2% of the computing time.

## 4.2 Numerical Experiments in 3D

In the previous 2d example, we did not apply grid adaption and the grid refining multilevel strategy for a better visualisation of the benefit achieved by the model hierarchy based approach. However, to solve the optimal boundary problem for glass cooling on a complex 3d geometry, the space-time adaptivity together with the grid refining multilevel strategy are essential. Since the combination of model hierarchy and multilevel strategy does not promise so much additional benefit, in this subsection we concentrate on the one model approach, using the grey scale model (10)-(14).

The involved PDAEs are solved by KARDOS3D (Erdmann et al., 2002). Different radiation models on a cube were already solved successfully with this software (Klar et al., 2005), although no optimisation was considered.

Unlike the previously considered case, the mean absorption coefficient  $\kappa$  in the grey scale problem is set to  $\kappa = 1.0$ . The other problem and model parameters are chosen as before. Since the arising PDAEs are solved adaptively in time and space, error tolerances have to be set. At the beginning of the optimisation process the local space and time error of the solution of the state equation should be smaller than  $1.0e - 02$ , while the local space error of the solution of the adjoint equation should be smaller than  $2.0e - 02$ . During the optimisation these tolerances are reduced as described in Figure 4. For stability reasons the tolerances are always halved, if a refinement is necessary. For the refinement criteria (38) and (39), the constants  $c_1 = c_2 = 1.0e - 2$  were chosen. The computations were done on a AMD Opteron DualCore 8218 with 3.0 GHz and 128 GB RAM with 533 MHz FSB.

Table 6: Optimisation protocol for grey scale model in three spatial dimensions

opt. iter.	target value	criticality measure	time nodes	space nodes		accumulated CPU time [s]
				State	Adjoint	
0	6.1996136e+02	2.561e+01	19	1399	1399	115
1	1.2240010e+02	1.644e+01	19	1399	1399	5 893
ref	1.2802449e+02	2.129e+00	31	1399	4897	11 867
3	1.2270402e+02	1.342e+00	31	1399	4897	45 845
4	1.2203427e+02	7.838e-01	31	1399	4897	83 894
ref	1.2076971e+02	1.294e+00	39	9192	9308	119 333
5	1.2035865e+02	1.170e+00	39	9192	9308	230 170
ref	1.1888023e+02	1.102e-01	71	67978	67978	356 458
6	1.1887778e+02	9.954e-02	71	67978	67978	2 398 655

In Table 6 the optimisation protocol of the glass cooling process modelled by the grey scale approximation can be seen. The target value and the criticality measure are not monotonically decreasing as in the case with fixed space and time grids. This is due to the adaptive refinement of these grids. Errors in the integration routine on coarser grids can lead to larger target value on finer grids. Since a good optimal control on a coarse grid usually isn't also a good optimal control on a finer grid, the criticality measure can increase after a grid refinement. After six optimisation iterations the space and time grids are quite fine and the computed optimal control can be trusted to approximate well the continuous optimal control.

The control iterates of the optimisation are shown in Figure 11(a). The convergence to the optimal control is quite fast. Most work has to be done around the transition from inactive to active control constraints at around  $t = 0.068$ .

In Figure 11(b) the temperature during the cooling process in four different points of the geometry is compared to the desired temperature  $T_d$ . These Points are  $Q_1 = (0, 0, 0)$  in the interior,  $Q_2 = (1, 1, -1)$  in a corner,  $Q_3 = (0, 0, -1)$  on a boundary facet and  $Q_4 = (0, -1, -1)$  on a boundary edge. The points on the edge and in the corner ( $Q_2$  and  $Q_4$ ) cool down uniformly and quicker than the points in the interior ( $Q_1$  and  $Q_3$ ).

In Figure 12 the terminal temperature distribution in the geometry resulting from the computed optimal control is compared to the one resulting from the initial control. While there are still great temperature differences between the corner and the interior for the initial control, the temperature distribution after an optimal cooling process is quite uniform and significantly lower.

In the last optimisation step, the local approximation errors in time and space of the state solution satisfy the quite strict tolerance  $6.25e - 04$  and the local approximation error in space of the adjoint solution satisfies the tolerance  $1.25e - 03$ . This results in an adaptive grid with 67978 nodes in space and 71 nodes in time. One can see that the last step consumes about 85% of the total computing time.

It was shown in Clever et al. (2010, 2012) that an optimisation using only the highest accuracy level

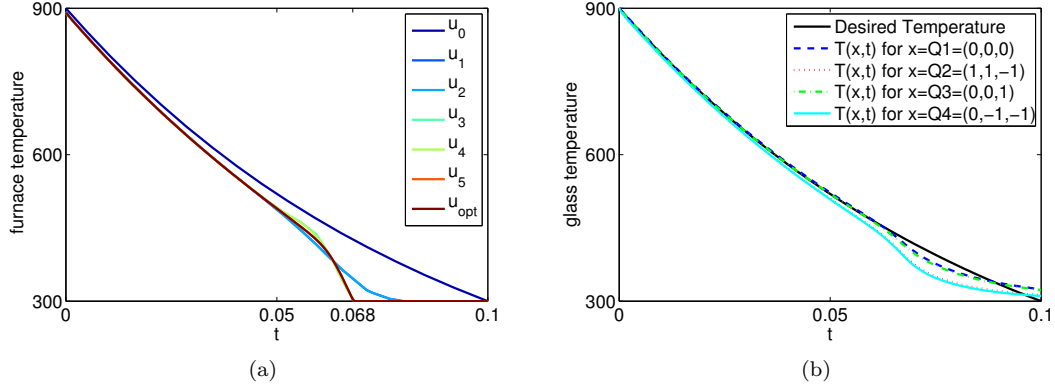


Figure 11: Control iterates and glass temperature profile at different points for the optimal control  
 In 11(a) the control iterates are displayed. A fast convergence to the optimal control can be observed. In 11(b) the temperature profile at four different points for the optimal control is compared with the desired temperature profile.

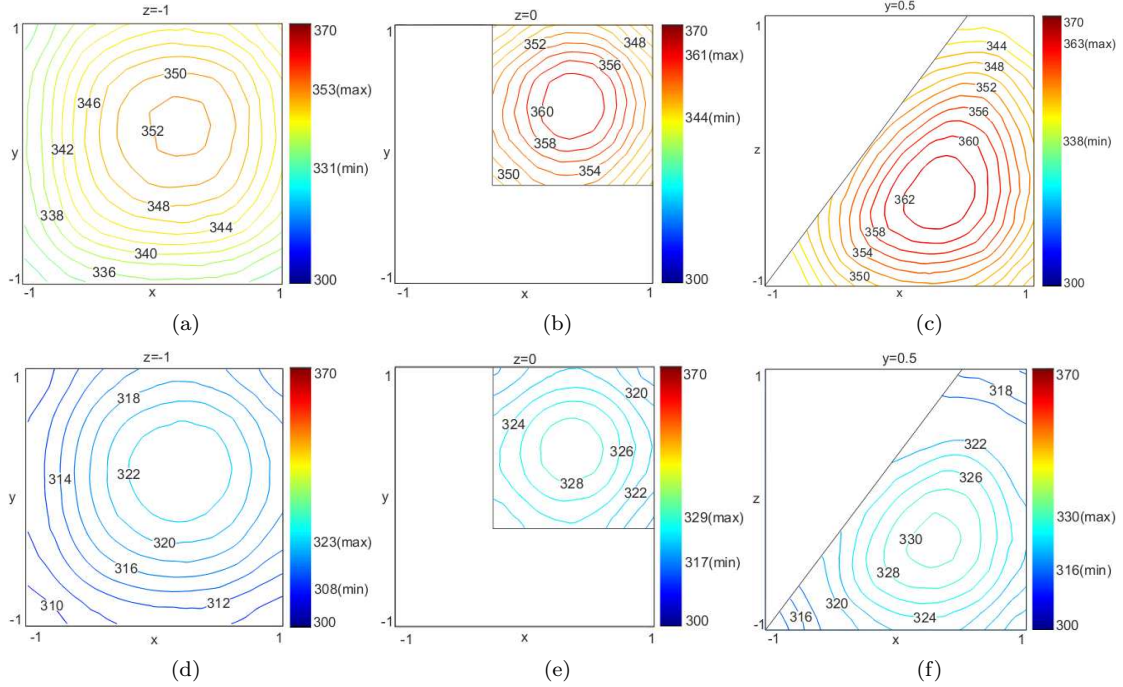


Figure 12: Terminal glass temperature distributions resulting from initial and optimal control  
 On top one can see the temperature distribution at the end of the cooling process resulting from the initial control and at the bottom the terminal temperature distribution resulting from the optimal control at different slices through the geometry. On the left  $z = -1$ , which is essentially the bottom of the geometry (12(a) and 12(d)), in the middle  $z = 0$  (12(b) and 12(e)) and finally on the right the slice is parallel to the  $y$ -axis with  $y = 0.5$  (12(c) and 12(f)).

is expected to take five times longer than the fully adaptive multilevel optimisation strategy. Since the multilevel optimisation took about 28 days, that would mean a computing time of about 140 days.

Summarising, it can be said, that the presented optimisation algorithm is capable of solving complex three dimensional problems. Further, we have presented a fully adaptive optimisation scenario for the glass cooling problem on a three dimensional computational domain. It can be seen, that here the grid refining multilevel strategy is of great advantage and makes the difference whether one can solve the optimisation problem in an acceptable time or not.

## 5 Conclusions

We have presented an adaptive multilevel and model hierarchy strategy to solve optimal control problems for glass cooling processes in two and three-dimensional geometries. Both strategies are useful to drastically reduce the computing time necessary to reach practically relevant accuracies. The model hierarchy based optimisation approach is especially attractive if no grid refinement options are available to solve the PDAE constraints. In this case, most of the work can be done on the basis of lower order and less expensive models. However, if adaptive discretisation schemes are used and therefore the last optimisation iteration is in general carried out on significantly fine meshes, then this advantage becomes less important.

Adaptive multilevel optimisation strategies based on successive improvement of the approximation property of the space-time discretisations perform remarkably robust and have the potential to solve even complex three-dimensional glass cooling problems within moderate time. Their great advantage is, that only a few optimisation steps have to be evaluated on the highest discretisation level. Needless to say, the two approaches presented can be applied to general PDAE-constrained optimal control problems.

## References

- Clever, D. and Lang, J. (2011). Optimal control of radiative heat transfer in glass cooling with restrictions on the temperature gradient, *Optim. Control Appl. Meth.*, *Published online in Wiley Online Library*, DOI: 10.1002/oca.984 .
- Clever, D., Lang, J., Ulbrich, S. and Ziems, J. C. (2010). Combination of an adaptive multilevel SQP method and a space-time adaptive PDAE solver for optimal control problems, *Procedia Computer Science* **1**: 1429–1437.
- Clever, D., Lang, J., Ulbrich, S. and Ziems, J. C. (2012). Generalized multilevel SQP-methods for PDAE-constrained optimization based on space-time adaptive PDAE solvers, in G. Leugering, S. Engell, A. Griewank, M. Hinze, R. Rannacher, V. Schulz, M. Ulbrich and S. Ulbrich (eds), *Constrained Optimization and Optimal Control for Partial Differential Equations*, International Series of Numerical Mathematics, Vol. 160, Basel, pp. 37–60.
- Erdmann, B., Lang, J. and Roitzsch, R. (2002). KARDOS-User’s Guide, Manual, Konrad-Zuse-Zentrum Berlin. **URL:** <http://www.zib.de/Numerik/software/kardos/>
- Farina, A., Klar, A., Mattheij, R. and A. Mikelić, N. S. (2010). *Mathematical Models in the Manufacturing of Glass*, Springer.
- Klar, A., Lang, J. and Seaïd, M. (2005). Adaptive solution of  $SP_N$ -approximations to radiative heat transfer in glass, *International Journal of Thermal Science* **44**: 1013–1023.
- Lang, J. (2001). *Adaptive multilevel solution of nonlinear parabolic PDE systems*, Springer.
- Lang, J. and Teleaga, D. (2008). Towards a fully space-time adaptive FEM for magnetoquasistatics, *IEEE Transactions on Magnetics* **44**,**6**: 1238–124.
- Lang, J. and Verwer, J. (2001). ROS3P - an accurate third-order Rosenbrock solver designed for parabolic problems, *BIT* **41**: 730–737.
- Larsen, E. W., Thömmes, G., Klar, A., Seaïd, M. and Götz, T. (2002). Simplified  $P_N$  approximations to the equations of radiative heat transfer and applications, *Journal of Computational Physics* **183**: 652–675.
- Pinnau, R. (2007). Analysis of optimal boundary control for radiative heat transfer modeled by the  $SP_n$ -system, *Communications in Mathematical Sciences* **5**(4): 951–969.
- Pinnau, R. and Thömmes, G. (2004). Optimal boundary control of glass cooling processes, *Mathematical Methods in the Applied Sciences* **27**(11): 1261–1281.
- Ziems, J. C. (2010). *Adaptive multilevel SQP-methods for PDE-constrained optimization*, PhD thesis, Technische Universität Darmstadt.
- Ziems, J. C. and Ulbrich, S. (2011). Adaptive multilevel inexact SQP-methods for PDE-constrained optimization, *SIAM J. Optim.* **21**: 1–40.